Precision Engineering 36 (2012) 153–157

Contents lists available at ScienceDirect

Precision Engineering

journal homepage: www.elsevier.com/locate/precision

Technical note

Periodic error quantification for non-constant velocity motion

Tony L. Schmitz*, Chirag Adhia, Hyo Soo Kim

Department of Mechanical and Aerospace Engineering, University of Florida, 237 MAE-B, Gainesville, FL 32611, United States

ARTICLE INFO

Article history:
Received 3 January 2011
Accepted 8 June 2011
Available online 28 June 2011

Keywords:
Interferometry
Heterodyne
Nonlinearity
Non-stationary
Fourier transform

ABSTRACT

This paper describes a procedure for analyzing non-stationary (variable frequency content) periodic error signals obtained during accelerating or decelerating motion. This capability is important due to the recent interest in real-time compensation of periodic error for precision positioning systems. In order to apply the spatial Fourier transform to the non-stationary signal, the constant time interval signals are resampled by linear interpolation using a constant spatial interval. Numerical and experimental results are provided for constant acceleration and sinusoidal motion profiles.

1. Introduction

Heterodyne displacement measuring interferometry enables displacement measurement for non-contact applications with high resolution and accuracy. However, there are a number of well-known error sources that can degrade the achievable accuracy [1–5]. These include cosine error, Abbe error, variations in refractive index, thermal deformations, beam shear, non-planar wavefronts, wavelength instability of the laser source, nonlinearity in the phase measuring electronics, and periodic error. While any of these error sources may dominate in a given situation (e.g., uncompensated refractive index changes for measurements in air often limit the accuracy), the focus of this study is periodic error. This error is superimposed on the measurement signal and occurs due to frequency mixing in the interferometer; see initial investigations by Fedotova [6], Quenelle [7], and Sutton [8]. Aspects of periodic error are:

- it is non-cumulative
- it repeats with each unit wavelength change in the optical path
- it depends on misalignments and imperfections in the optical setup
- it is characterized as first and second order errors which typically appear simultaneously on the measurement signal.

In this paper, the time-domain frequency variation for periodic error during acceleration or deceleration is explored. An approach for identifying the individual magnitudes of first and second order periodic error during non-constant velocity motion is presented. This is a relevant topic due to the recent efforts in measuring and compensating periodic error in real-time for arbitrary motion profiles, particularly for position feedback in semiconductor manufacturing [9–12].

2. Periodic error frequency content

First order periodic error has a spatial wavelength, Λ_1, equal to the light wavelength, λ, divided by the interferometer's fold factor, *FF*, which describes the number of light passes through the interferometer; see Eq. (1). The spatial wavelength of second order periodic error, Λ_2, is half that of first order periodic error; see Eq. (2). When a position signal, *x*, which includes periodic error is sampled during constant velocity motion, the time-domain periods for first and second order errors are constant. Fig. 1 displays simulated periodic error with a first order magnitude of 1.2 nm and second order magnitude of 0.8 nm for a velocity of 100 mm/s; the sampling frequency is 10 MHz and $\lambda = 633$ nm. The interferometer configuration for this simulation includes a polarizing beam splitter and a retroreflector in both the measurement and reference paths, so the fold factor is 2. The constant period error observed in Fig. 1 is exploited during "velocity scanning", where the Fourier transform frequency content of constant velocity motion is interrogated to identify the first and second order periodic error magnitudes [13,14].

$$\Lambda_1 = \frac{\lambda}{FF} \tag{1}$$

$$\Lambda_2 = \frac{\lambda}{2FF} \tag{2}$$

* Corresponding author. Tel.: +1 352 392 8909; fax: +1 352 392 1071.
E-mail address: tschmitz@ufl.edu (T.L. Schmitz).

0141-6359/$ – see front matter © 2011 Elsevier Inc. All rights reserved.
doi:10.1016/j.precisioneng.2011.06.004

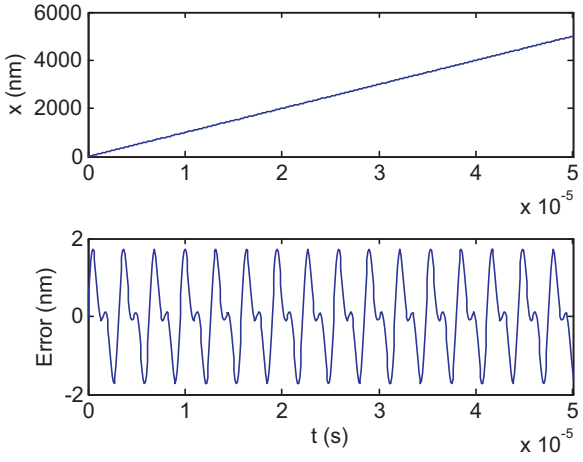

Fig. 1. (Top) Displacement with a constant velocity of 100 mm/s. (Bottom) Simulated periodic error for constant velocity motion with a first order magnitude of 1.2 nm and second order magnitude of 0.8 nm.

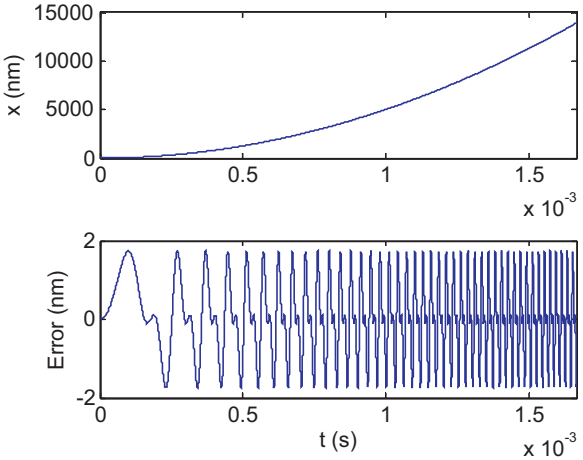

Fig. 2. (Top) Displacement with a constant acceleration of 10 m/s^2. (Bottom) Simulated periodic error for constant acceleration motion with a first order magnitude of 1.2 nm and second order magnitude of 0.8 nm.

For accelerating (or decelerating) motion, however, the period varies with velocity. Fig. 2 shows the periodic error for a constant acceleration (from rest) of 10 m/s^2 to a velocity of 100 mm/s. In this case, the periods for the first and second order errors decrease (i.e., their frequencies increase) in the time-domain representation. The first and second order magnitudes are again 1.2 nm and 0.8 nm, respectively, and the sampling frequency is 10 MHz.

Because the frequency content varies with time, the signal in Fig. 2 is non-stationary and the standard Fourier transform cannot be applied. Common alternatives for analyzing non-stationary signals include the short time Fourier transform[1] and the wavelet transform. However, with a simple resampling of the data in Fig. 2, the standard Fourier transform can still be applied. This is described in Section 3.

3. Resampling analysis for non-stationary periodic error

A new plotting format for the time-domain Fig. 2 aids in analyzing the non-stationary periodic error. In Fig. 3 the time axis is replaced by position. This demonstrates that periodic error is only non-stationary in the time domain, not the spatial domain. However, the sampling interval, δx, in the spatial domain varies with velocity (because the sampling interval was constant in the time domain, but the velocity is non-constant). This is also shown in Fig. 3.

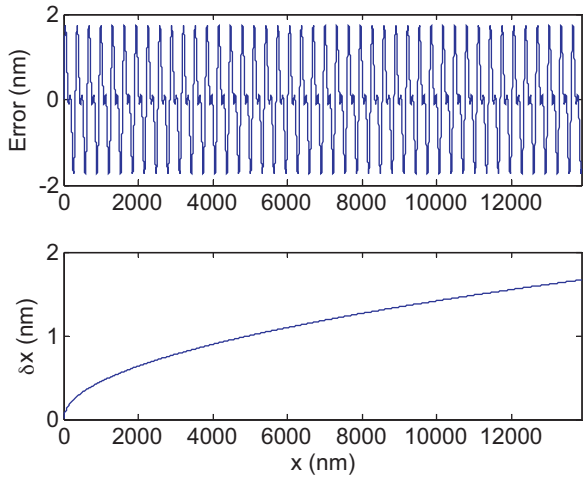

Fig. 3. (Top) The periodic error is stationary in the spatial domain. (Bottom) The sampling interval varies.

In order to apply the Fourier transform in the spatial domain, the data points must be equally spaced. This is accomplished by resampling the signal in Fig. 3 using linear interpolation (or other interpolation scheme). The only requirement is that the new sampling period must be small enough to avoid aliasing of the first and second order errors. For a fold factor of two and wavelength of 633 nm, a sampling interval of a few nanometers is sufficient. Fig. 4 shows the beginning and end of the original signal with the samples identified by squares; the sampling interval is variable. The resampled data (circles) with a new sampling interval of 5 nm is also included, but is offset vertically by 0.5 nm for plotting purposes. At the beginning of the motion, the velocity is low so the original signal has closely-spaced samples. At the end, the velocity is high and the sampling interval is larger.

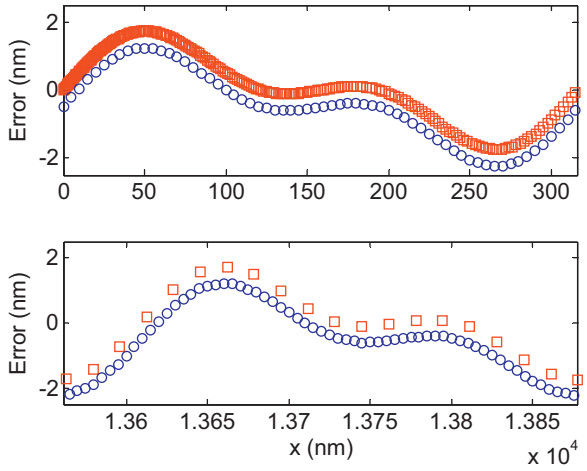

Fig. 4. (Top) Original (squares) and resampled (circles) data at the beginning of the motion where the velocity is low. (Bottom) Data at the end of the motion where the velocity is high.

[1] In the short term Fourier transform, the signal is divided into small segments that can each be considered to be stationary. A window function is used to isolate the segments.

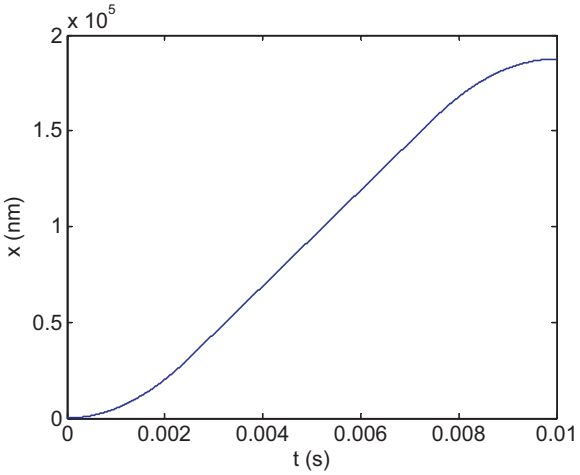

Fig. 5. Constant acceleration motion profile.

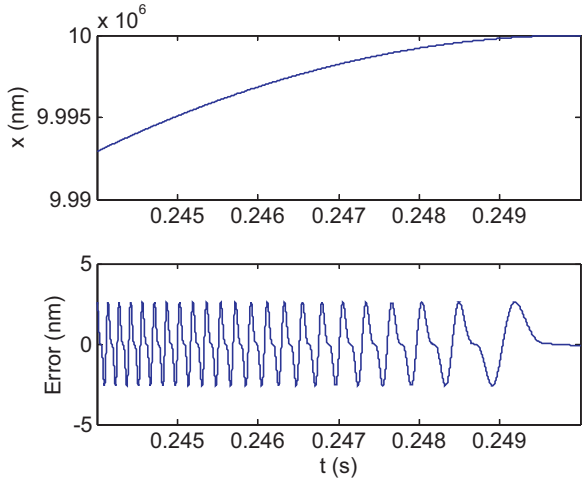

Fig. 7. Analysis section for sinusoidal motion profile.

3.1. Constant acceleration example

For this example, a constant acceleration of 10 m/s^2 was commanded (maximum velocity of 25 m/s). The motion profile is shown in Fig. 5. The non-stationary periodic error was resampled using a spatial interval of 2 nm. The pre-defined first and second order magnitudes were 3 nm and 1 nm, respectively, and the sampling frequency was 10 MHz. The spatial Fourier transform was calculated using a sampling frequency, f_s, of:

$$f_s = \frac{1}{\delta x} = \frac{1}{2} \quad \text{nm}^{-1}. \tag{3}$$

The result is provided in Fig. 6, where the frequency axis was normalized to error order by multiplying by $\lambda/2$.

3.2. Sinusoidal motion example

In this example, a sinusoidal motion profile was commanded with a magnitude of 10 mm and frequency of 1 Hz. The first quarter of the sine wave was considered; Fig. 7 shows the analysis section from the end of the first quarter. The pre-defined first and second order periodic error magnitudes were 2 nm and 1 nm, respectively. The non-stationary error was resampled using a spatial interval of 1 nm. The corresponding Fourier transform is provided in Fig. 8.

4. Experimental results

To verify the resampling analysis technique, displacement data were collected using the heterodyne interferometer setup shown in Fig. 9. The two-frequency laser head emitted the laser beams with nominally orthogonal polarizations that passed through a half-wave plate (HWP) to a non-polarizing beam splitter (80% transmission/20% reflectance), which split it into two parts: the reference beam, which was used as the phase reference in the phase measuring electronics, and the measurement beam, which traveled to the interferometer. The reference beam was collected using the reference fiber optic pick-up, which included a linear polarizer oriented at 45 deg relative to the nominally orthogonal linear polarizations for the two heterodyne frequencies, and formed the reference signal. The measurement beam passed through the polarizing beam splitter (PBS) where one frequency was directed into the reference arm of the interferometer with the stationary retroreflector, while the other frequency was directed into the measurement arm with the moving retroreflector (*FF* = 2 for this setup). The frequency in the measurement arm was Doppler-shifted during motion of the moving retroreflector. The two laser beams recombined at the PBS and were directed to the mixing linear polarizer (LP). The interference signal was then collected by the measurement fiber optic pick-up. The HWP was used to artificially vary the rotational misalignment between the PBS and the two nominally

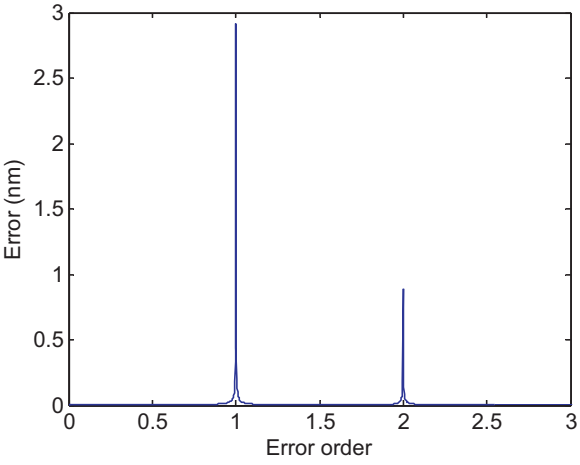

Fig. 6. Spatial Fourier transform of the resampled data for the constant acceleration example.

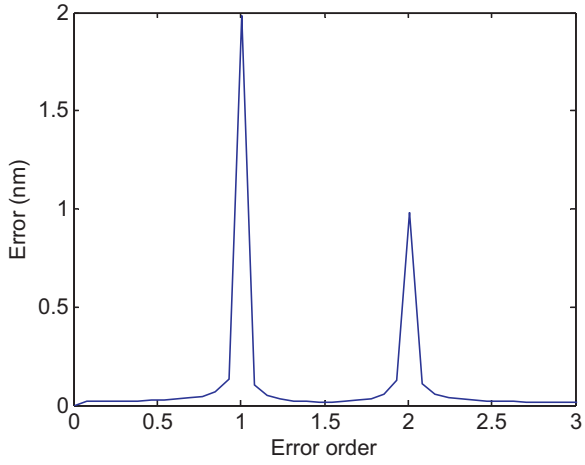

Fig. 8. Spatial Fourier transform of the resampled data for the sinusoidal motion example.

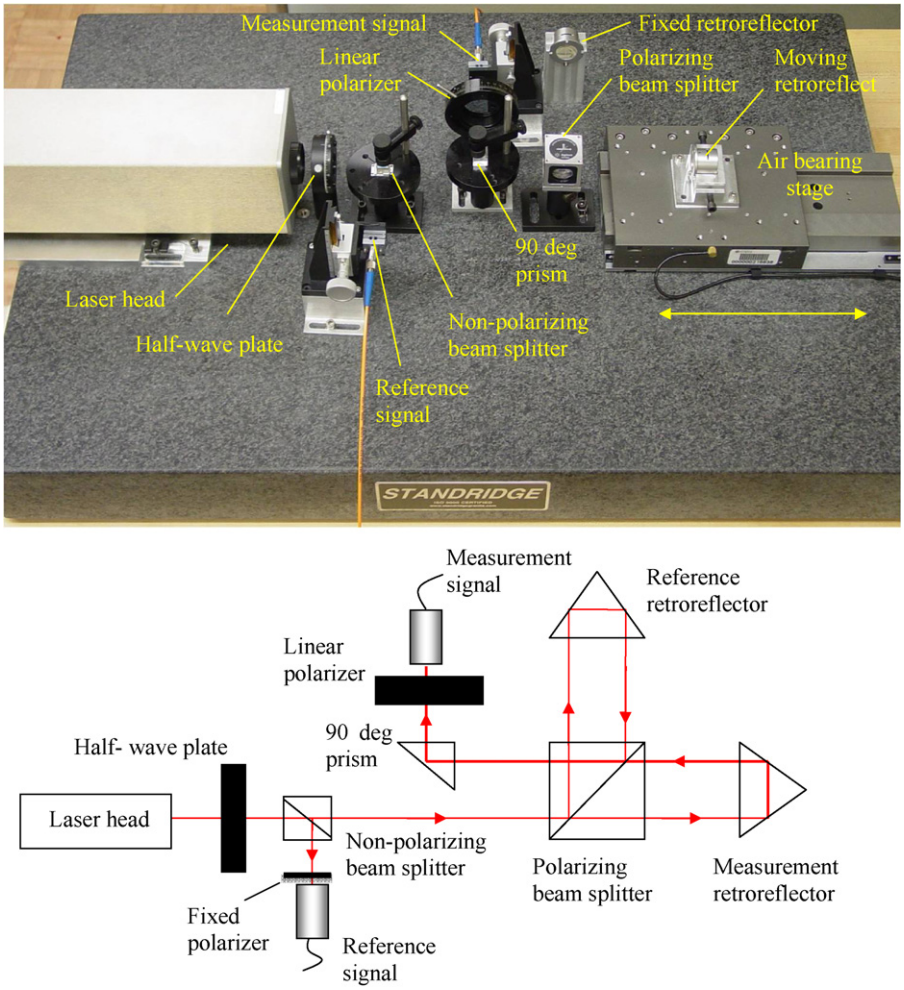

Fig. 9. (Top) Photograph of the heterodyne interferometer experimental setup. (Bottom) Schematic of the setup, where the linear polarizer and half-wave plate each had a rotational degree of freedom about the beam axis to vary the level of periodic error.

orthogonal, linearly polarized frequencies that make up the source laser beam. The orientation of the mixing LP was also adjusted to vary the periodic error magnitudes.

A sinusoidal motion profile with a magnitude of 0.1 mm and frequency of 2 Hz was commanded for the air bearing stage which carried the moving retroreflector. The HWP and LP were adjusted to give significant first order error with small second order error for demonstration purposes. A section of the measurement signal from the beginning of the sinusoid is displayed in Fig. 10 (312.5 kHz sampling frequency). The periodic error was isolated by subtracting

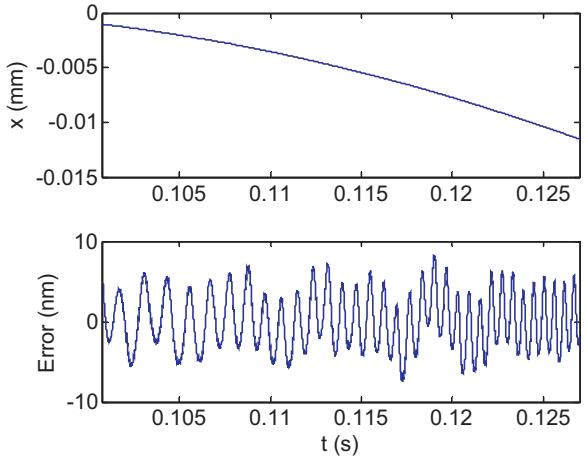

Fig. 10. (Top) A non-constant velocity section of the displacement signal from the sinusoidal motion profile. (Bottom) The periodic error was isolated by subtracting the least-squares best fit polynomial from the macro-scale motion.

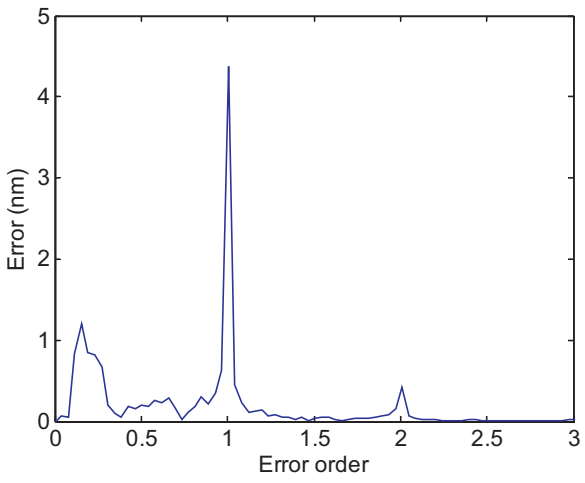

Fig. 11. Fourier transform of the non-stationary periodic error from Fig. 10 after resampling.

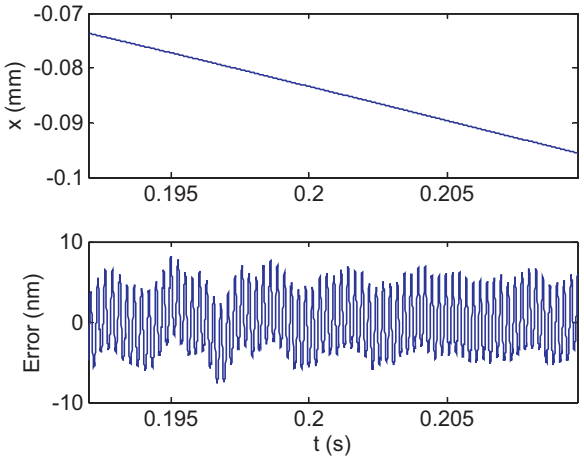

Fig. 12. (Top) A constant velocity section of the displacement signal from the sinusoidal motion profile. (Bottom) The periodic error was isolated by subtracting the least-squares best fit polynomial from the macro-scale motion.

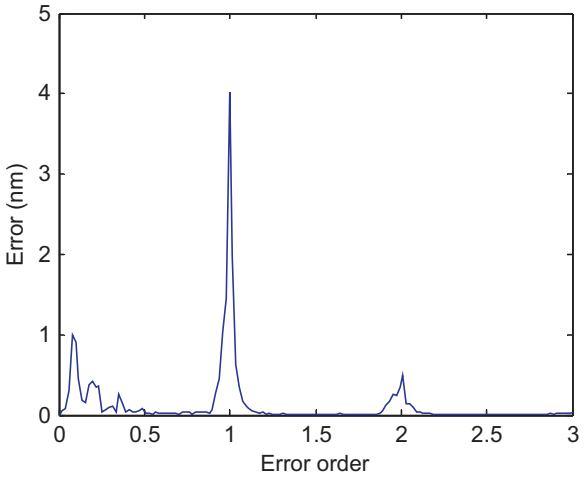

Fig. 13. Fourier transform of the stationary periodic error from Fig. 12 (no resampling).

the least-squares best fit polynomial; this result is also shown. It is observed that some low-frequency content remained due to small departures of the actual motion from the commanded sinusoid. As shown in the numerical examples, the error signal is non-stationary, where the sampling interval varies from 0.5 nm to 2 nm for the analysis section. The signal was resampled using a spatial interval of 2 nm and the spatial Fourier transform was calculated. The result is provided in Fig. 11. The first order error magnitude is 4.2 nm and the second order error magnitude is 0.4 nm.

For comparison purposes, a section of the measurement signal with approximately constant velocity was also analyzed. This section is shown in Fig. 12, where the mean sampling interval is 4 nm (0.3 nm standard deviation). The Fourier transform was calculated without resampling. The result is provided in Fig. 13, where the first order error magnitude is 4.0 nm and the second order error magnitude is 0.5 nm. These results agree with the non-stationary results in Fig. 11. In both Figs. 11 and 13, the residual low-frequency content from the time-domain signals after subtracting the least-squares best fit polynomial is observed as spectral content below the first order periodic error peak.

5. Conclusions

Due to the interest in real-time compensation of periodic error in precision motion applications, such as semiconductor manufacturing, it is necessary to analyze non-constant velocity profiles to determine the efficacy of the compensation algorithm. This analysis is complicated by the nature of the periodic error signals. Because periodic error is characterized by constant spatial periods (one each for first and second order error), the signal is non-stationary for accelerating/decelerating motions. It was shown that a resampling of the data by interpolation enables the spatial Fourier transform to be applied for determination of the residual periodic error magnitudes.

Acknowledgement

This work was partially supported by Agilent Technologies, Santa Clara, CA.

References

[1] Bobroff N. Residual errors in laser interferometry from air turbulence and nonlinearity. Applied Optics 1987;26:2676–82.
[2] Bobroff N. Recent advances in displacement measuring interferometry. Measurement Science and Technology 1993;4:907.
[3] Estler WT. High-accuracy displacement interferometry in air. Applied Optics 1985;24:808–15.
[4] Schmitz T, Evans C, Davies A, Estler WT. Displacement uncertainty in interferometric radius measurements. CIRP Annals – Manufacturing Technology 2002;51:451–4.
[5] Schmitz T, Kim H. Monte Carlo evaluation of periodic error uncertainty. Precision Engineering 2007;21:251–9.
[6] Fedotova G. Analysis of the measurement error of the parameters of mechanical vibrations. Measurement Techniques 1980;23:577–80.
[7] Quenelle R. Nonlinearity in interferometric measurements. Hewlett–Packard Journal 1983;34:10.
[8] Sutton C. Non-linearity in length measurement using heterodyne laser Michelson interferometry. Journal of Physics E: Scientific Instruments 1987;20:1290–2.
[9] Chu D, Ray A. Nonlinearity measurement and correction of metrology data from an interferometer system. In: Proceedings of 4th euspen international conference. 2004. p. 300–1.
[10] Schmitz T, Chu D, Houck III L. First-order periodic error correction: validation for constant and non-constant velocities with variable error magnitudes. Measurement Science and Technology 2006;17:3195–203.
[11] Schmitz T, Chu D, Kim HS. First and second order periodic error measurement for non-constant velocity motions. Precision Engineering 2009;33:353–61.
[12] Ellis J, Baas M, Spronck JW, Munnig Schmidt RH. Errors in measurement and compensation algorithms for periodic nonlinearity correction. In: Proceedings of the 25th annual meeting of the American Society for Precision Engineering (ASPE). 2010.
[13] Patterson S, Beckwith J. Reduction of systematic errors in heterodyne interferometric displacement measurement. In: Proceedings of the 8th international precision engineering seminar (IPES). 1995. p. 101–4.
[14] Badami V, Patterson S. A frequency domain method for the measurement of nonlinearity in heterodyne interferometry. Precision Engineering 2000;24:41–9.